Journal of Theoretical and Applied Information Technology
15th April 2023. Vol.101. No 7

ISSN: 1992-8645 www.jatit.org E-ISSN: 1817-3195

# ADAPTIVE SCALING IN DEEP CONVOLUTIONAL NEURAL NETWORKS FOR COVID-19 IDENTIFICATION IN X-RAY IMAGES

**MOHAMMED SIDHEEQUE[1], P. SUMATHY[2], ABDUL GAFUR. M[3]**

[1,2] School of Computer Science,Engineering & Applications, Bharathidasan University, Tamil Nādu, India.

[3] KMCT College of Engineering for emergingTechnology, Kerala, India

Email: [1]mohammedsidheeque@gmail.com, [2]sumathy.p@bdu.ac.in, [3]abdulgafurm@gmail.com

**ABSTRACT**

For X-ray image COVID-19 identification, researchers turn to deep convolutional neural networks (CNNs). Deep convolutional neural networks (CNNs) may struggle with detecting objects in noisy X-ray pictures. To enhance COVID-19 identification in noisy X-ray pictures without the need for any pre-processing for noise reduction, we offer a unique CNN technique using adaptive convolution to increase the resilience of a deep CNN against impulsive noise. Based on the standard CNN architecture, this method adds an impulsive an adaptive convolution layer, adaptive scaling layer, and a noise-map layer. Furthermore, we enhanced the deep CNN's generalization by using a learning-to-augment technique on noisy X-ray pictures. Twenty-nine hundred and three chest X-ray photos have been gathered, including those showing Healthy and COVID 19. GoogleNet, SqueezeNet, ResNet18, MobileNetv2, ShuffleNet, ResNet50 and EfficientNetb0 are just some of the pre-trained networks that have had their design tweaked to improve their resilience against impulsive noise. Verification using a distorted X-ray ResNet50 trained with the suggested noise-robust layers and learning-to-augment technique outperformed the state-of-the-art method by 2%.

**Keywords**: *Covid-19 Classification, Adaptive Resize, Data Augmentation, Noise, Adaptive Convolution*

## 1. INTRODUCTION

The COVID-19 epidemic has created widespread economic disruption and healthcare system backlogs. including, but not limited to, critical care units. In its final stages, COVID-19 illness necessitates a prolonged stay in critical care. The diagnosis of COVID-19 is sought via the use of computed tomography (CT) scans or X-rays, the Polymerase Chain Reaction (PCR) test, and the fast antigen test [1, 2]. Constructed tomography (CT) pictures are the result of integrating X-ray images collected from various angles of the patient's body to reveal the desired region of interest. If the patient is in the early stages of the illness or the viral load is low, the PCR test used to identify COVID-19 may provide a negative result. Obtaining CT scans of the patient at this time is crucial for determining the presence of COVID-19. The infancy of nucleic acid detection technology, variations in detection rates across manufacturers, and improper clinical sampling, as noted by [3], may all contribute to a false negative PCR result. It was determined by Fang et al. (2020) that the sensitivity of the PCR test for the early detection of COVID-19 was 71%, whereas the sensitivity of the detection of COVID-19 by using CT scans was 98%. When it comes to identifying COVID-19, CT scans are favored over X-rays. Since X-rays may not reveal the characteristic ground glass pattern in the lung during the first stages of COVID-19 illness.

A convolutional neural network (CNN) is a powerful method for classifying images [4-10], and it has found applications in many different industries. In 2017, CNNs of several forms were widely employed for COVID-19 detection in medical pictures. Examples include the work of Jia et al. The enhanced MobileNet has been utilized to identify COVID-19 along with other respiratory diseases.

Accuracy rates of 98.5 percentage points on chest X-rays and 98.4 percentage points on CT scans were attained using these methods. Similar to what was done by Thakur et al. [11], COVID-19 was detected using deep CNN applied to X-ray images. This model was trained to make binary classifications using a database of X-ray images that included both 1813 instances of COVID-19 and 1845 healthy controls. Classification accuracy of

98.23 percent, F-measure of 98.16 percent, and receiver operating characteristics of 0.99 were all attained by using this technique. To categorize X-ray pictures [11], [13] created a CNN architecture that combines the U-Net and Fractal blocks and they showed that their model outperformed state-of-the-art methods like Xception [14], ResNet50 [15] and Inception-ResNetV2 [16]. Furthermore, its model was readily trainable on chest X-ray pictures.

Whale Optimizer and Grey Wolf Optimizer were used to fine-tune the CNNs that were a part of the ensemble model. When testing the model on chest X-ray images for differentiation between healthy, COVID and viral patients, they were able to obtain a multiclass classification accuracy of 98.8%. In order to identify COVID-19 in chest X-rays, [17 - 20] presented a hybrid technique including wavelet transform CN. In this study, we used deep learning to extract features from X-ray images after first enhancing and segmenting the images. Combines the benefits of CNN with the DWT [21 – 25]. After that, we used a recursive feature removal procedure to pick out the characteristics that were the most relevant and had the fewest redundant data points. Finally, a bagging approach based on a random forest was used to the COVID-19 detection job, and its results showed a classification accuracy of 98.5%. COVID-19 and healthy images are shown in Fig. 1.

We present a unique CNN architecture that includes a built-in layer like adaptive scaling, noise-map and an adaptive convolution layer in order to boost the CNN's resistance to impulsive noise. This framework also includes an adaptive convolution layer.

The following is a synopsis of our technical contributions:

1. To increase a CNN's job performance, we incorporate a noise-map layer module into the CNN architecture, which produces a binary noise-map identifying the spatial position of noisy and normal pixels in an image? In addition to saving time, this module makes it such that noise-reduction processing of photographs isn't necessary beforehand.

2. At the front end of a convolutional neural network (CNN), we also present an adaptive picture resizing module that we've built into the CNN framework. This module has the ability to concurrently remove noise and resize the image.

## 2.RELATED WORK

Deep learning may be classified into unsupervised, supervised, and semi-supervised learning depending on the training dataset's labels are shown in Table. 1. Images are all tagged via supervised learning, and the model is tuned using these image-label pairings. A probability score will be generated for each testing picture based on the model's optimum parameters [15]. It's possible to use unsupervised learning to discover patterns or hidden data structures without providing any labels to the model beforehand. Throughout the long term, various kinds of works have been laid out to recognize COVID-19 infection according to an unmistakable viewpoint. Scientists all over the planet attempted to concoct a model that can efficiently group this sickness considering a short measure of time.

Different exchange learning draws near stood out on account of inadequate measure of coronavirus affected lung pictures. In this part, a concentrate on the current deals with COVID-19 classification will completely depict with suitable portrayal what's more, portrayal. Various categories of chest images are shown in Fig. 2.

Noise Free

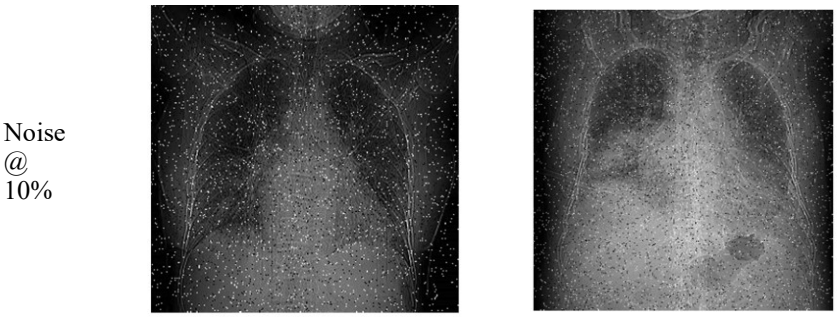


(a) (b)

Fig.1 (a) COVID-19 and (b) healthy

(a) (b) (c) (d)

**Fig. 2 Chest X Ray Images a) Covid 19, b) Bacterial Pneumonia c) Viral Pneumonia d) Normal**

*Table 1: Deep learning based classification*

| Author, Year | CNN Technique | Image | Accuracy (%) | Remarks |
|---|---|---|---|---|
| Vedika Gupta,2022 [1] | AlexNet | 2905 images | 98 | Concatenation-based CNN model. |
| Muhammed Yildirim,2022 [2] | MobilenetV2, Efcientnetb0, and Darknet53 | COVID and Non-COVID images of X-Rays. | 99.05, 97.1 | NCA approach has been used to decrease the size of obtained feature maps. |
| Wassim Zouch,2022 [3] | VGG and ResNet | COVID and Non-COVID images of X-Rays. | 99.35, 96.77 | Transfer learning |
| Lokeswari Venkataramana,2022 [5] | DenseNet-161, ResNet-18 | Bacterial - 3001<br>Viral - 1656<br>COVID- 1281 | 97.4 | SMOTE (Synthetic Minority Oversampling Technique |
| Ivanoe De Falco, 2021 [6] | DEREx | Covid-19 3,616<br>Normal 10,192 | 97.52 | Automatically extract explicit knowledge under the form of a set of IF-THEN rules |
| Priyanka Saha, 2021 [7] | Concat_CNN | COVID and Non-COVID images of X-Rays. | 96.31 | Concatenation-based CNN model |

| | | | | |
|---|---|---|---|---|
| Arman Haghanifar, 2021 [8] | COVID-CXNet | 1326 images of COVID-19, 5,000 normal, 4,600 images of patients with CAP | 87.88 | CheXNet model is utilized to develop COVID-CXNet |
| Asmaa Abbas, 2020 [9] | DeTraC model | 11 SARS, 80 normal, 105 Covid | 93.1 | A class decomposition mechanism achieved by DeTraC model |
| Daphna Keidar, 2021 [10] | Ensemble (ResNet34, ResNet50, ResNet152) | A total of 2427 frontal from 1384 patients, 360 with COVID-19 and 1024 negative | 90.3 | Implemented a nearest-neighbours algorithm that uses DNN-based image embedding's to retrieve the images |
| Vishu Madaan, 2021 [11] | XCOVNet | 196 COVID-19, 388 Covid –ve, 366 other diseases | 98.44 | facing a serious need to find out the severity level of the infection too |
| Sifat Ahmed, 2021 [12] | HRNet | 521 COVID-19, 12 ARDS | 99.26 | 98.53% sensitivity, and 98.82% specificity |

## 3. PROPOSED MODEL

### 3.1 Impulse noise in X-ray Images

Impulse noise, often known as salt and pepper noise, is known to frequently contaminate chest X-ray pictures [15-21]. This corruption is often brought on by a broken X-ray receiver, bit errors in the transmission of an X-ray picture, or erroneous memory locations in the hardware. The impulse noise causes changes in the pixel intensities in a medical image to become distorted, which results in highest or lowest possible value for the grey level it contains. The noise caused by the bipolar impulse is shown in Eq. (1).

$$h(x) = \begin{cases} h_a & x=a \\ h_b & x=b \\ 0 & else \end{cases} \quad (1)$$

When the quality of the X-ray pictures is significantly reduced due to impulse noise, it is difficult to identify COVID-19 in the tainted X-ray image. In order to solve this issue, Lu et al. devised a technique for the elimination of impulse noise that makes use of a weighted neighbor pixel-based gain factor adaptation [21]. Gray level variation is used as the basis for sorting and grouping all of the pixels inside the window that has been chosen for this procedure. After the pixels have been grouped together, the distribution ratio and median value for each group are computed so that an estimate of the values of the gain factors may be made. These gain factors will ultimately be put to use as weights for surrounding pixels that will take the place of the pixel that was contaminated by noise. A filter that can eliminate impulsive noise from pictures was developed by Arora et al. [25], and it makes use of a fuzzy switching median filter in addition to the idea of information sets. This approach works in two stages: the first stage identifies the pixels that have been tainted by the impulse noise, and the second stage applies a filter to the noisy pixels by making use of an adaptive switching criteria. An impulse noise removal filter that utilizes the min-max average pooling approach was suggested by Satti et al. [24]. When compared to their noisy counterparts, the recovered medical pictures exhibited an increase in peak signal-to-noise ratio (PSNR) of 1.2 decibels due to the use of this method.

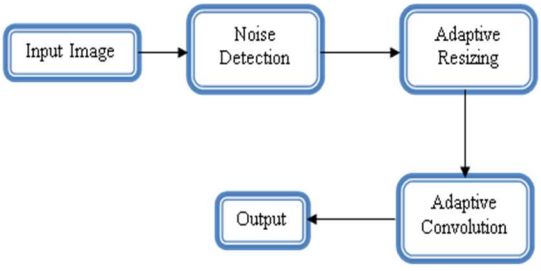


*Fig.3 Proposed Method Flow*

Journal of Theoretical and Applied Information Technology
15th April 2023. Vol.101. No 7

ISSN: 1992-8645 www.jatit.org E-ISSN: 1817-3195

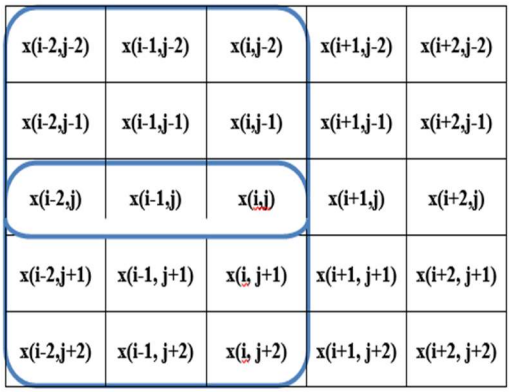


(a)

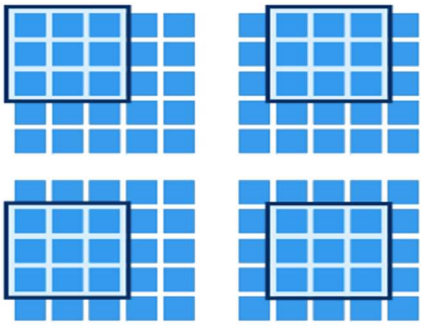

(b)

*Fig. 4 a) The 5 × 5 window b) 3 × 3 sub-windows*

### 3.2 Detecting Impulse Noise

The study of an image's local statistical features might be used in order to identify the pixels that have been distorted as a result of impulsive noise. In this study, we apply a switching technique-based fuzzified degree to determine which pixels in a picture are free of noise and which ones include noise.

**Step 1.** Let x signify a processing window that has been picked. This window is a tiny area of the damaged picture that is centered at position $(i, j)$ . The processing window is 5 pixels wide and 5 pixels tall in its entirety. The processing window is then subdivided into sub-windows with overlaps of 3 pixels by 3 pixels as shown in Fig.4.

**Step 2.** Absolute mean differences are calculated using

$$M_i = Median\ (S_l) \qquad (2)$$

Where $S_l$ indicates $lth$ sub-window for $l$ = 1, 2,…,9

In Eq. (2), the median values of each of the nine sub-windows are ranked from lowest to highest as shown in Eq.(3).

$$\vec{S} = [\overline{s_1}, \overline{s_2}, \overline{s_3}, \overline{s_4}, \overline{s_5}, \overline{s_6}, \overline{s_7}, \overline{s_8}, \overline{s_9}] \qquad (3)$$

$$H_1 = Mean(x) - x(i,j) \qquad (4)$$

$$H_2 = \sum_{p=2}^{9}(s_k - s_{k-1}) \qquad (5)$$

where, $H_1$ and $H_2$ are noisy pixels in an image.

**Step 3.** In this stage of the process, we used fuzzy logic to determine whether or not the current pixel contains noise as shown in Fig. 5. In order to do this, we give each pixel a degree of impulsiveness that we determine by utilizing fuzzy gradient values. The difference between the gradients is analyzed and then categorized as nondeterministic characteristics so that noisy pixels may be distinguished from edges (Large or Small) are represented in Eq.(4) and (5).

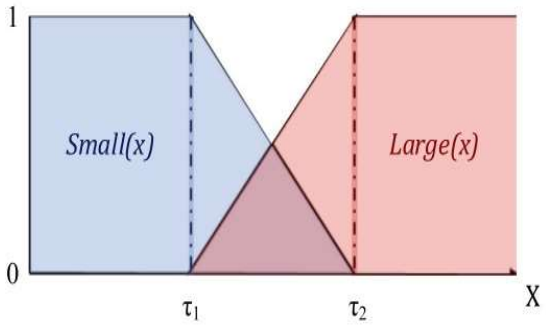


*Fig. 5 Fuzzy Membership function*

**Step 4.** The fourth stage involves using a switching strategy that is based on a fuzzified degree in order to locate the noisy pixels. After that, the noise map for a whole picture is created by employing the method described above to analyze each pixel in the image in question. This results in the creation of the noise map.

### 3.3 Adaptive resizing

In most cases, the dimensions of the pictures that are fed into a CNN are all the same (for example, 244 pixels by 244 pixels). In addition, if a model is pre-trained, the dimensions

of the input photos that are used for fine-tuning should match those of the images that the model was pre-trained on. Because the models that we employ in this study have already been trained, we need to adjust our X-ray pictures so that their dimensions match the dimensions of the images that were used in the pre-training process. In this study, rather of utilizing a standard interpolation-based technique to resizing photographs, we employed an adaptive image resizing strategy, which is more resilient on noisy images. This is because adaptive image resizing takes into account the inherent characteristics of each individual image. In order to explain how the process behind this resizing strategy works, we will resize two noisy photos of 64 by 64 pixels, one with a low noise density and the other with a high noise density, into noise-reduced images of 8 by 8 pixels.

We use the adaptive resizing approach so that we may circumvent this problem. This method ensures that noisy pixel values are not carried over to the picture that has been scaled. When we have finished resizing pictures by utilizing the associated noise-map, we next resize the noise-map itself such that the size of the updated noise-map is the same as the size of the updated image.

### 3.4 Adaptive convolution

Our convolution layer is designed to be adaptive so that it can better withstand the effects of picture noise. A CNN's convolution layer will often be responsible for the generation of a new feature map. Incorporating noise-map into the convolution kernel, which is a binary map, helps to prevent the noisy pixel value from being propagated forward through the network.

### 3.5 Output Layer

To begin, the initial dataset is split into two distinct halves called folds. After that, an

The amount of time it takes for the procedures that are used to enhance the quality of noisy X-ray pictures to run is of utmost importance, particularly for the point-of-care equipment that are used in clinical settings. In most cases, X-ray pictures that have been ruined by impulse noise are improved using a process that consists of two parts. During the first stage, it is determined if a pixel contains noise or not. The quality of the X-ray pictures is improved throughout the subsequent and final step of the process.

impulse noise and a Gaussian noise were added to the X-ray pictures in each fold using a noisy data generator in their own right. The Bayesian optimizer searches for optimal values for various parameters, and the augmenters use those values to produce fresh X-ray pictures. After that, each fold receives its own individual feeding into the kid CNN models. The controller improves the performance of better policies while maintaining the performance of weaker policies by using the output of child CNNs. The Bayesian optimization method is what the controller uses in order to get the best possible results from the augmentation policies.

## 4. PROPOSED METHOD

During the training phase, we solely used the learning-to-augment technique with noisy data, but during the testing phase, we only utilized the suggested noise-robust method. Our model is able to acquire knowledge from both noise-free and noisy data thanks to this overarching technique. Setting the impulse noise density is the first step in the learning-to-augment technique that makes use of the noisy X-ray pictures. The X-ray pictures that are produced by the noisy data generator are distorted because of the impulse noise. The Bayesian optimization method determines the most effective strategy for data enhancement. The proposed method flow is represented in Fig. 3.

## 5. RESULTS AND DISCUSSIONS

Experiments using deep learning were run on a computer equipped with an Intel Core i7–7700HQ processor running at 2.81 GHz, 32 gigabytes of random access memory (RAM), and an Nvidia GTX 1070 graphics processing unit (GPU) with 8 gigabytes of video memory (VRAM). When it came time to fine-tune the pre-trained CNNs, we used stochastic gradient descent (SGD) with a learning rate of 0.001.

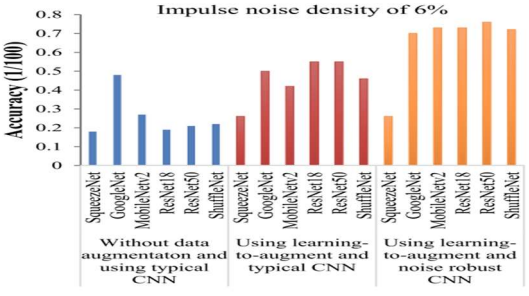


*Fig. 6 COVID-19 accuracy by various method*

*Table: 2 Covid 19 Detection Error percentage*

| CNN Models | Impulse noise density | | | | | | |
|---|---|---|---|---|---|---|---|
| | 1% | 2% | 5% | 6% | 8% | 9% | 10% |
| | 0.92 | 0.93 | 0.93 | 0.94 | 0.95 | 0.95 | 0.95 |
| GoogleNet | 0.69 | 0.82 | 0.84 | 0.85 | 0.85 | 0.87 | 0.88 |
| | 0.68 | 0.83 | 0.83 | 0.85 | 0.85 | 0.87 | 0.88 |
| | 0.61 | 0.62 | 0.62 | 0.63 | 0.63 | 0.65 | 0.66 |
| SqueezeNet | 0.46 | 0.52 | 0.57 | 0.58 | 0.61 | 0.63 | 0.65 |
| | 0.39 | 0.41 | 0.41 | 0.42 | 0.42 | 0.43 | 0.44 |
| | 0.72 | 0.75 | 0.8 | 0.85 | 0.85 | 0.86 | 0.9 |
| ResNet18 | 0.41 | 0.47 | 0.49 | 0.66 | 0.71 | 0.71 | 0.82 |
| | 0.37 | 0.37 | 0.39 | 0.39 | 0.39 | 0.4 | 0.4 |
| | 0.64 | 0.83 | 0.88 | 0.91 | 0.91 | 0.94 | 0.95 |
| MobileNetv2 | 0.39 | 0.4 | 0.43 | 0.51 | 0.52 | 0.58 | 0.58 |
| | 0.35 | 0.38 | 0.38 | 0.39 | 0.39 | 0.4 | 0.41 |
| | 0.79 | 0.89 | 0.9 | 0.9 | 0.9 | 0.91 | 0.92 |
| ShuffleNet | 0.48 | 0.51 | 0.54 | 0.6 | 0.6 | 0.67 | 0.67 |
| | 0.35 | 0.38 | 0.39 | 0.39 | 0.41 | 0.41 | 0.42 |
| | 0.78 | 0.79 | 0.84 | 0.86 | 0.91 | 0.92 | 0.92 |
| ResNet50 | 0.62 | 0.62 | 0.61 | 0.58 | 0.58 | 0.55 | 0.53 |
| | 0.34 | 0.35 | 0.36 | 0.36 | 0.37 | 0.37 | 0.38 |

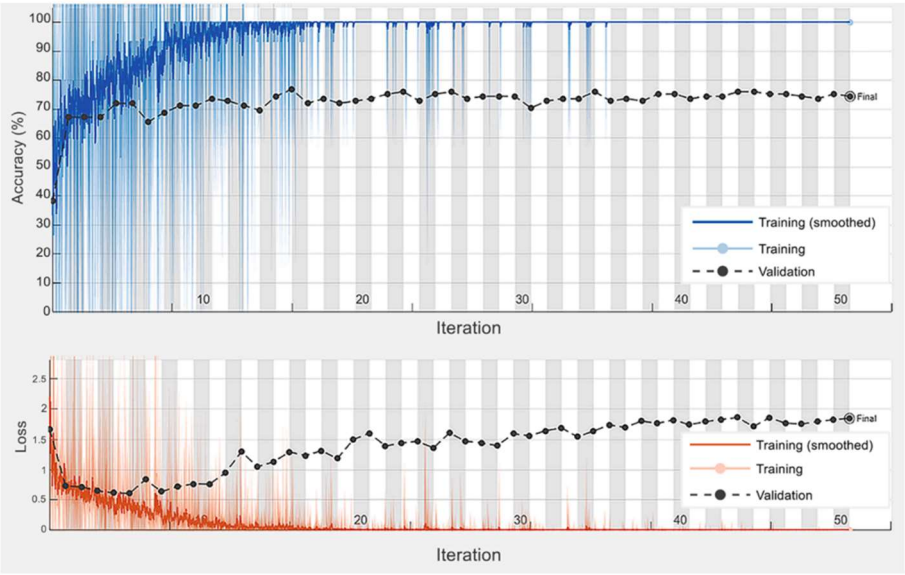


*Fig.7 Training and validation Accuracy and Loss*

## 6. CONCLUSION

The system that we have presented incorporates a number of innovative image processing components. Making use of a switching approach that is determined by the degree to which an image has been fuzzed up, the noise-map layer module has the ability to efficiently increase detection inside a noisy picture. The adaptive resizing layer module has the capability to do interpolation-based picture scaling while concurrently removing noisy pixels from the image. This is accomplished via the adaptive convolution operation. We went one step further and integrated the learning-to-augment technique for automated augmentation of training pictures. This led to an improvement in the deep models' ability to generalize to X-ray images. We added our innovative modules to a number of deep CNNs that had already been trained. In addition, the suggested model does not need any pre-treatment for the removal of impulsive noise; rather, noise reduction occurs on-the-fly as a result of our innovative modules, which speeds up the categorization of noisy X-rays. As a result, the findings of this study imply that the proposed method has the potential to be very efficient in classification tasks, even when applied to noisy data, and has the potential to increase the generalization of deep CNN. In the not too distant future, one of our goals is to investigate whether or not our noise-resistant CNN is able to enhance the performance of classification tasks using high-density noise-corrupted X-ray pictures.

## REFERENCES:

[1] M.K. Hasan, M.T. Jawad, K.N.I. Hasan, S.B. Partha, M.M.A. Masba, S. Saha, M. A. Moni, COVID-19 identification from volumetric chest CT scans using a progressively resized 3D-CNN incorporating segmentation, augmentation, and class-rebalancing, Inform. Med. Unlocked (2021), 100709.

[2] G. Jia, H.-K. Lam, Y. Xu, Classification of COVID-19 chest X-Ray and CT images using a type of dynamic CNN modification method, Comput. Biol. Med. 134 (2021), 104425.

[3] A.M. Ismael, A. S¸engür, Deep learning approaches for COVID-19 detection based on chest X-ray images, Expert Syst. Appl. 164 (2021), 114054.

[4] A. Jahanbakhshi, Y. Abbaspour-Gilandeh, K. Heidarbeigi, M. Momeny, A novel method based on machine vision system and deep learning to detect fraud in turmeric powder, Comput. Biol. Med. 136 (2021), 104728.

[5] K. R. Devi, S. Suganyadevi, S. Karthik and N. Ilayaraja, "Securing Medical Big data through Blockchain technology," 2022 8th International Conference on Advanced Computing and Communication Systems (ICACCS), 2022, pp. 1602-1607, doi: 10.1109/ICACCS54159.2022.9785125..

[6] A J Dickinson, C. Hintschich, Clinical manifestations, in: Graves' Orbitopathy, Karger Publishers, 2017, pp. 1–25.

[7] Suganyadevi, S., Seethalakshmi, V. CVD-HNet: Classifying Pneumonia and COVID-19 in Chest X-ray Images Using Deep Network. Wireless Pers Commun (2022). https://doi.org/10.1007/s11277-022-09864-y

[8] S. Suganyadevi, K. Renukadevi, K. Balasamy and P. Jeevitha, "Diabetic Retinopathy Detection Using Deep Learning Methods," 2022 First International Conference on Electrical, Electronics, Information and Communication Technologies (ICEEICT), 2022, pp. 1-6. https://doi.org/10.1109/ICEEICT53079.2022.9768544.

[9] Suganyadevi, S., Seethalakshmi, V. & Balasamy, K. A review on deep learning in medical image analysis. Int J Multimed Info Retr (2021). https://doi.org/10.1007/s13735-021-00218-1

[10] Balasamy K, Suganyadevi S (2021) "A fuzzy based ROI selection for encryption and watermarking in medical image using DWT and SVD" Multimed Tools Appl 80, 7167–7186, https://doi.org/10.1007/s11042-020-09981-5.

[11] R Citro, G Pontone, M Bellino, et al., Role of multimodality imaging in evaluation of cardiovascular involvement in COVID-19, Trend. Cardiovasc. Med. 31 (1) (2021) 8–16.

[12] M J Horry, S Chakraborty, M Paul, et al., COVID-19 detection through transfer learning using multimodal imaging data, IEEE Access 8 (2020) 149808–149824.

[13] Jianshe Shi, Yuguang Ye, Daxin Zhu, Lianta Su, Yifeng Huang, Jianlong Huang, Comparative analysis of pulmonary nodules segmentation using multiscale residual U-Net and fuzzy C-means clustering, Comput. Method. Program. Biomed. 209 (2021) 106332.

[14] T J Brinker, A Hekler, J S Utikal, et al., Skin cancer classification using convolutional neural networks: systematic review, J. Med. Internet Res. 20 (10) (2018) e11936.

[15] R. Girshick, Fast r-cnn, in: Proceedings of the IEEE international conference on computer vision, 2015, pp. 1440–1448.

[16] H C Shin, H R Roth, M Gao, et al., Deep convolutional neural networks for computer-aided detection: CNN architectures, dataset characteristics and transfer learning, IEEE Trans. Med. Imaging 35 (5) (2016) 1285–1298.

[17] Balasamy, K., Krishnaraj, N. & Vijayalakshmi, K. Improving the security of medical image through neuro-fuzzy based ROI selection for reliable transmission. Multimed Tools Appl 81, 14321–14337 (2022). https://doi.org/10.1007/s11042-022-12367-4.

[18] S Hershey, S Chaudhuri, D P W Ellis, et al., CNN architectures for large-scale audio classification, in: 2017 ieee international conference on acoustics, speech and signal processing (icassp), IEEE, 2017, pp. 131–135.

[19] Gopalakrishnan T., Ramakrishnan S., Balasamy K., Murugavel A.S.M., Semi fragile watermarking using Gaussian mixture model for malicious image attacks, 2011 World Congress on Information and Communication Technologies,2011: 120 – 125..

[20] L Yu, B Li, B. Jiao, Research and implementation of CNN based on TensorFlow, IOP Conference Series: Materials Science and Engineering, 490, IOP Publishing, 2019.

[21] Z Lu, Y Bai, Y Chen, et al., The classification of gliomas based on a pyramid dilated convolution resnet model, Pattern Recognit. Lett. 133 (2020) 173–179.

[22] Krishnasamy, B., Balakrishnan, M., Christopher, A. (2021). A Genetic Algorithm Based Medical Image Watermarking for Improving Robustness and Fidelity in Wavelet Domain. In: Satapathy, S., Zhang, YD., Bhateja, V., Majhi, R. (eds) Intelligent Data Engineering and Analytics. Advances in Intelligent Systems and Computing, vol 1177. Springer, Singapore. https://doi.org/10.1007/978-981-15-5679-1_27

[23] Suganyadevi S, Shamia D, Balasamy K (2021) An IoT-based diet monitoring healthcare system, for women. Smart Healthc Syst Des Secur Priv Asp. https://doi.org/10.1002/9781119792253.ch8.

[24] L Wen, X Li, L. Gao, A transfer convolutional neural network for fault diagnosis based on ResNet-50, Neur. Comput. Applica. 32 (10) (2020) 6111–6124.

[25] K He, X Zhang, S Ren, et al., Deep residual learning for image recognition, in: Proceedings of the IEEE conference on computer vision and pattern recognition, 2016, pp. 770–778.